



Generating long-term stable squeezed states via multiple pump noise suppression

LI GAO,^{1,†} SHAOPING SHI,^{1,3,†}  BO LU,¹ LI-ANG ZHENG,¹ LONG TIAN,^{1,2} WEI LI,^{1,2} 
YAJUN WANG,^{1,2}  AND YAOHUI ZHENG^{1,2,*} 

¹State Key Laboratory of Quantum Optics Technologies and Devices, Institute of Opto-Electronics, Shanxi University, Taiyuan 030006, China

²Collaborative Innovation Center of Extreme Optics, Shanxi University, Taiyuan 030006, China

³ssp4208@sxu.edu.cn

*yhzheng@sxu.edu.cn

[†]These authors contributed equally to this work.

Received 20 May 2025; revised 22 June 2025; accepted 22 June 2025; posted 23 June 2025; published 21 July 2025

Pump power fluctuations are a critical factor in limiting the long-term stability of quantum sensing light sources. However, existing laser power stabilization techniques fail to efficiently address power fluctuations caused by downstream beam-pointing noise coupling. Here, we propose an optimized suppression scheme of pump power fluctuations that integrates a passive second harmonic process and active feedback control, achieving multiple noise suppression of both pointing and intensity noise in the pump field. Within the measurement time of 8.5 hours, we achieve a quantum sensing light source with a squeezing factor of 10.0 dB and its fluctuations below 0.4 dB. The proposed approach effectively boosts the long-term stability of the quantum squeezing source, thus paving a solid way for expanding the utilization of squeezing sources within the realm of quantum precision measurement. © 2025 Optica Publishing Group. All rights, including for text and data mining (TDM), Artificial Intelligence (AI) training, and similar technologies, are reserved.

<https://doi.org/10.1364/OL.568435>

Over the past few decades, squeezed states have found widespread applications across multiple fields due to their unique quantum properties, including quantum metrology [1,2], quantum sensing [3–6], and quantum communication [7–9]. In particular, in the field of quantum precision measurement, the application of squeezed states has proven crucial for detecting weak signals, such as gravitational waves. In 2019, LIGO first introduced squeezed vacuum states into the laser interferometer, increasing the interferometer's measurement sensitivity and successfully capturing weaker astronomical events [10]. Currently, squeezed vacuum states have become a general technique of ground-based gravitational-wave observatories, continuously speeding up the drive to upgrade [11–14]. Integrated with waveguide [15] and on-chip technique [16], squeezed states of light will undoubtedly have a bright future. Practical application does also require the generation system involved to be stable at the timescale of several hours, as a by-product, driving a squeezing spectrum extension to the lower frequency band [17–20].

The generation of squeezed states typically relies on techniques such as optical parametric down-conversion [21] and four-wave mixing [22], with optical parametric down-conversion being one of the most common methods for preparing squeezed states. The semi-monolithic optical parametric oscillator (OPO) represents an ideal solution for generating high-quality squeezed vacuum states. This is attributed to its minimized optical surfaces, which effectively reduce intracavity losses [23], and its sufficient degrees of freedom for active control. The squeezed vacuum states generated using this method currently hold the record for the highest achieved squeezing levels [24]. However, enhancing measurement sensitivity using squeezed states is not solely dependent on a high squeezing factor but is also closely related to their stability and control precision. Compared to singly-resonant OPOs, a major advantage of doubly-resonant OPOs is their ability to extract cavity length locking error signals via the pump field [25]. Additionally, doubly-resonant OPOs have lower threshold pump power [26,27], allowing for the generation of a higher squeezing factor at lower pump powers. By using a coherent and frequency-shifted auxiliary beam, the relative phase of the squeezed vacuum states can also be accurately controlled [28]. Previous research has demonstrated the close correlation between pump fields and the long-term stability of squeezed light sources [29,30]. While the coherent control scheme decoupled from cavity length has been proposed, the relative phase of the light field is still susceptible to environmental disturbances, leading to phase fluctuations. On the timescale of several hours, such fluctuations eventually degrade the squeezing level of the squeezed vacuum state and worsen the stability of phase locking.

In this paper, we investigate the additional pointing fluctuations introduced during the phase-locking process. By developing a corresponding theoretical model, we analyze the influence of pointing fluctuations on the downstream resonant cavity output field. Theoretical calculations demonstrate that, in comparison with the OPO, second harmonic generation (SHG) exhibits lower sensitivity to pointing fluctuations. Furthermore, the gain saturation effect in SHG further suppresses pointing fluctuations, while the remaining pointing noise is converted into intensity noise by the SHG cavity. We propose a modified

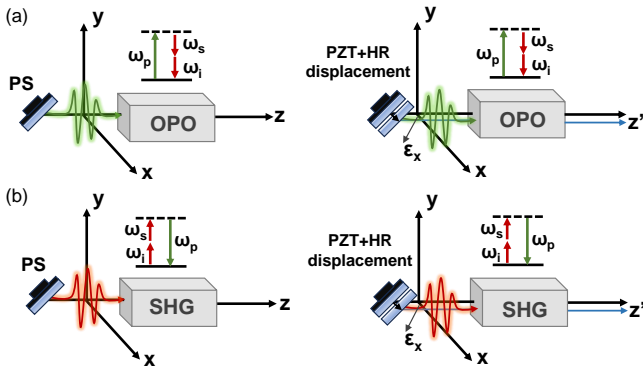


Fig. 1. Schematic diagram of beam coupling with the resonator. The green line represents the pump light, while the red line represents the fundamental light. (a) OPO, optical parametric oscillator; (b) SHG, second harmonic generation.

experimental scheme that utilizes the SHG cavity for pre-suppressing noise in the pump field, in conjunction with a downstream laser power feedback control system, to achieve comprehensive suppression of multiple noise sources—including both pointing and intensity noise. Finally, we generate a squeezed vacuum state with the squeezing level of approximately 10.0 dB, with fluctuations of below 0.4 dB during an 8.5-hour active locking process. To our knowledge, this is the minimum value of squeezing noise fluctuation over 8.5 hours. Combined with frequency stabilization schemes and an automatic relocking system, we expect to generate a squeezed light source with lower fluctuations and longer locking time.

The preparation of squeezed states is a highly phase-sensitive process. The introduction of a coherent control scheme [31] effectively addresses the phase-locking issue of squeezed vacuum states. When the optical field is subjected to external perturbations, such as vibrations or temperature drifts, the phase shifter functions as an actuator to adjust the relative phase between the beams. Typically, the phase shifter in the pump path is used to adjust the squeezed angle. However, during the process of responding to the phase-locked feedback loop, the initially perfectly matched pump beam for the OPO will experience a displacement as shown in Fig. 1(a).

For the OPO, any degree of beam misalignment reduces the coupling efficiency of the pump mode [32,33]. We introduce the misalignment and mismatch parameters into the field amplitude of the pump field, establishing a corresponding theoretical model. Compared to axial displacement (pointing fluctuations), the effect of radial displacement (beam waist variation) on the pump coupling efficiency is negligible. For the same axial displacement, a smaller beam waist results in greater fluctuations in the coupling efficiency of the light field. The detailed analysis is shown in Supplement 1.

Continuous changes in the pump mode alter the pump factor within the OPO cavity, ultimately degrading the squeezing level and long-term stability of the squeezed state. Therefore, pointing fluctuations are one of the key factors limiting the stable output of the OPO. To mitigate the impact of pointing noise, we compare the effects of phase shifters on different optical cavities. As shown in Fig. 1(b), the phase shifter is placed before the SHG cavity and acts on the fundamental light. Since the SHG conversion efficiency is dependent on the incident fundamental light, the output pump power of the SHG is not simply linearly

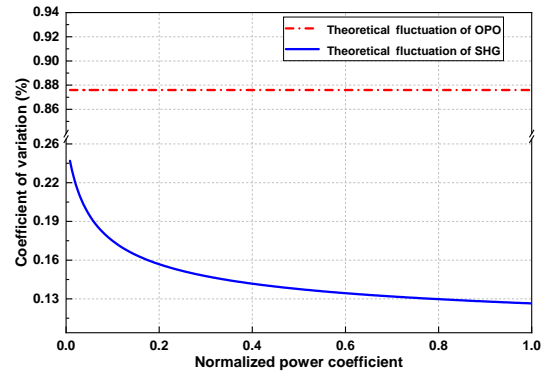


Fig. 2. Comparison of the output power fluctuations for different optical cavities. The x-axis represents the ratio of the actual incident power to the maximum incident power, while the y-axis denotes the ratio of the standard deviation to the mean of the power.

related to the incident fundamental light power [34,35]. It can be expressed as:

$$\eta_{SHG} = E_{NL} \times P_c^2 / P_{in}, \quad (1)$$

$$P_c = \frac{P_{in} \times T}{[1 - \sqrt{(1-T)(1-L)(1-\Gamma \times P_c)}]}^2, \quad (2)$$

where P_c represents the circulating power of the fundamental light within the SHG, T is the transmittance of the input coupling mirror for the fundamental light, L represents the round-trip loss of the fundamental light within the cavity, and $\Gamma = E_{NL} + \Gamma_{abs}$ denotes the total sum of all nonlinear losses.

As shown in Fig. 2, we obtain the fluctuation characteristics of the cavity output power when the phase shifter is applied to SHG or OPO by calculating the coefficient of variation. The red and blue curves represent the fluctuation trends for the OPO and SHG, respectively. Due to the larger beam waist of the fundamental light (43.0 μm) compared to the pump light (28.0 μm), the power fluctuation of the SHG is minor for the same pointing fluctuation. As the normalized power coefficient increases, the power fluctuation of the SHG decreases and gradually stabilizes. We attribute this behavior to the saturation effect of the SHG conversion efficiency. The detailed analysis is shown in Supplement 1.

A schematic of our experimental setup is illustrated in Fig. 3. The laser source is a nonplanar ring oscillator (NPRO) laser at 1064 nm. About 1.5 W laser power transmits through a mode cleaner (1064 MC1) for spatial-mode filtering and polarization purifying of the downstream experiment. At the first beam splitter (BS) behind the 1064 MC1, approximately 100 mW of reflected light is passed through two acousto-optic modulators (AOMs) to generate the sideband field, which serves as an auxiliary beam to control the squeezed angle. A small portion of the transmitted light is retained as the local oscillator (LO), meanwhile the remaining light is primarily used for SHG to provide the 532-nm pump light. An additional mode cleaner (1064 MC2) is positioned before the optical path of the LO and the SHG, acting as an optical low-pass filter and spatial mode cleaner. The structures of SHG and OPO are similar, both comprising a piezoelectric-driven concave mirror and a PPKTP crystal, forming a semi-monolithic cavity. The crystal dimensions are 1 mm \times 2 mm \times 10 mm, with refractive indices of 1.83 at 1064 nm and

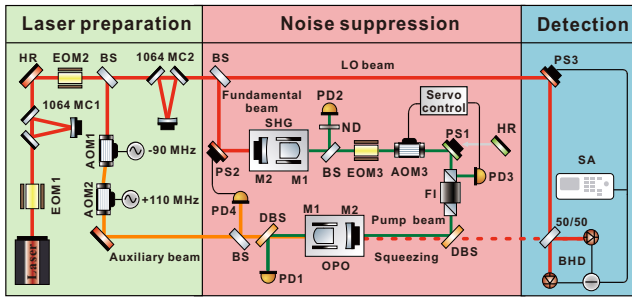


Fig. 3. Schematic of experimental setup. AOM, acousto-optic modulator; BHD, balanced homodyne detector; BS, beam splitter; DBS, dichroic beam splitter; EOM, electro-optic modulator; FI, Faraday isolator; HR, high-reflective mirror; MC, mode cleaner; M1/M2, end face; ND, neutral density filter; OPO, optical parametric oscillator; PD, photoelectric detector; PS, phase shifter; SA, spectrum analyzer; SHG, second harmonic generation.

Table 1. Detailed Parameters of SHG and OPO

Parameter	SHG	OPO
ROC_{M1}	12.0 mm	12.0 mm
R_{M1}	HR > 99.99% @ 1064; AR < 0.2% @ 532	HR > 99.99% @ 1064; HR > 99% @ 532
ROC_{M2}	30.0 mm	25.0 mm
R_{M2}	R = 91% \pm 1% @ 1064; HR > 99% @ 532	R = 85% \pm 1% @ 1064; R = 97.5% \pm 0.5% @ 532
Cavity length	37.0 mm	31.0 mm
Cavity waist	43.0 μ m @ 1064	40.4 μ m @ 1064; 28.0 μ m @ 532
Singly/Doubly resonant	Singly	Doubly

1.89 at 532 nm. The specific structural parameters, such as the radius of curvature (ROC) and reflectivity (R) of the SHG and OPO, are detailed in Table 1. Additionally, EOM1 and EOM2, located in the main optical path, are used to lock the cavity lengths of MC1 (MC2) and the SHG. To avoid signal crosstalk, EOM3 is placed separately in the pump path to independently lock the OPO cavity length.

To suppress the impact of pointing noise on the long-term stability of the squeezing, we use the phase shifters (PS1 and PS2) as actuators in the phase-locked feedback control loop for comparative validation. A triangular wave scan signal is employed to drive the PS1 or PS2 for simulating the pointing fluctuation induced by phase drift. The pump light fluctuations transmitted by the OPO and the pump light fluctuations output by the SHG are measured by injecting equal optical power into a low-noise photodetector (PD1/PD2), as shown in Figs. 4(a) and 4(b). It is evident that scanning the PS in front of the optical cavity causes periodic fluctuations in the output power. With the input normalized power coefficient fixed at 0.8, the coefficients of variation for the OPO and SHG output powers are 0.89% and 0.13%, respectively, with peak-to-peak fluctuations of 3.71% and 1.00%. The coefficients of variation are in excellent agreement with the theoretical model.

As illustrated in Figs. 4(c) and 4(d), we also generate the corresponding violin plots [36] by normalizing the data and grouping them into samples, in which per sample includes 1000

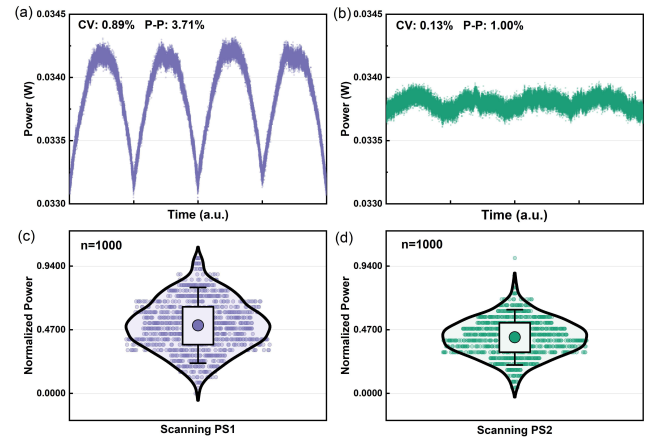


Fig. 4. Difference in fluctuation of output pump power between the OPO and SHG.

data points. The data points within the plots depict the distribution of the sampled data, meanwhile the shape of the violin plots corresponds to the probability density distribution of the data. Compared to Fig. 4(c), the shorter length of the violin plot in Fig. 4(d) indicates a higher data concentration within a smaller range. The box plot in the center of each figure reflects the average value of the data, with the vertical axis corresponding to the normalized power. The length of the box indicates that 50% of the sampled data falls within this range. It can be seen that scanning PS2 in front of the SHG cavity under the same conditions significantly suppresses the pointing fluctuations' impact on the output power. The results demonstrate that the pointing fluctuations introduced by the phase shifter can be efficiently suppressed by the SHG process.

During the long-term quantum noise measurement process, the entire optical platform is placed inside a light-shielded black sealed enclosure. We control the squeezed angle by feeding back the reflected field from the OPO to PS2. Additionally, we replace the PS1 in the pump path with a high-reflective mirror and implement a multi-noise suppression scheme for the pump light using SHG and an AOM-based active feedback control system. The squeezed vacuum state generated by the OPO is separated from the pump light using a dichroic beam splitter and subsequently combined with the LO beam to enter the balanced homodyne detection (BHD) system. The AC signal from the BHD is split into two paths: one for directly measuring the optical field noise and the other for demodulating the detection phase of the squeezed state, enabling long-term stability measurements of the maximum squeezing level.

The BHD measurements are shown in Fig. 5, with a steady pump power of 7.8 mW. The black dashed line in Fig. 5 corresponds to shot noise, while the pink line represents the measured squeezing. Under continuous, uninterrupted measurements, it is clearly shown that the squeezed state remained stable at 10.0 dB for approximately 8.5 hours. To observe the variation in squeezing during the lock-in time, we present a histogram of the measured squeezing data in the inset (a) of Fig. 5. The squeezing level fluctuates by no more than 0.4 dB within 8.5 hours, with the squeezing level remaining above 10.0 dB for the majority of the time. These results directly indicate the stability of the generated quantum squeezing source. Furthermore, we provide the squeezing measurements at the analysis frequency of 1 MHz in the inset (b) of Fig. 5, where the pink (blue) line repre-

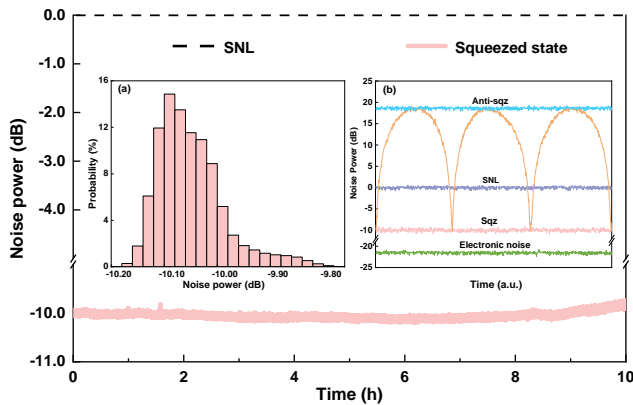


Fig. 5. Long-term measurement of the squeezed vacuum state. The analysis frequency is 500 kHz, RBW = 300 kHz, and VBW = 1 kHz. The black dashed line represents shot noise; the pink line represents the measured squeezing. The inset (a) shows the histogram of the squeezing measurement within an 8.5-hour period. The inset (b) shows the squeezing measurement at the analysis frequency of 1 MHz.

sents the squeezing (anti-squeezing) noise measurements under the same pump power. It can be observed that this aligns with the squeezing level measured during the long-term measurement process.

It is noteworthy that the system's stability is not only related to the pump source but also closely linked to the laser source stability. Loss of lock in MC1 causes total instability across all loops of the squeezed light source. Therefore, optimizing the frequency drift of the laser is a key focus for our future work. The results reported in this paper provide that, by stabilizing the laser source and optimizing the locking loop, the squeezed light source will enable more stable output over extended periods.

In conclusion, we have proposed an experimental scheme for reducing the intensity and pointing noise of the pump light. By comparing the theoretical model with experimentally measured power fluctuations, we quantitatively assessed the impact of pointing fluctuations on the output field. Furthermore, the unique saturation effect of SHG inherently suppressed a portion of the environment-induced pointing noise, providing excellent temporal stability for subsequent experiments. Combined with noise conversion and power stabilization schemes, the setup was able to maintain a squeezing level better than 10.0 dB for 8.5 hours, with fluctuations not exceeding 0.4 dB. Achieving this in a non-vacuum-isolated environment is particularly challenging. In the future, by integrating frequency stabilization and automatic relocking schemes, we aim to maintain even superior stability over longer measurement times. Our work provides a new theoretical framework and technological approach for the design and application of highly stable squeezed light sources, with significant potential in fields such as quantum precision measurement and quantum communication.

Funding. National Natural Science Foundation of China (62225504, 62027821, U22A6003, 12304399, 12174234, 12274275, 62375162); Key RD Program of Shanxi (202302150101015); Fundamental Research Program of Shanxi Province (202303021212003, 202303021224006).

Disclosures. The authors declare no conflicts of interest.

Data availability. Data underlying the results presented in this paper are not publicly available at this time but may be obtained from the authors upon reasonable request.

Supplemental document. See Supplement 1 for supporting content.

REFERENCES

- J. Aasi, J. Abadie, B. Abbott, *et al.*, *Nat. Photonics* **7**, 613 (2013).
- G. Ortolano, A. Paniate, P. Boucher, *et al.*, *Light Sci. Appl.* **12**, 171 (2023).
- M. J. Yap, J. Cripe, G. L. Mansell, *et al.*, *Nat. Photonics* **14**, 19 (2020).
- M. I. Kolobov and P. Kumar, *Opt. Lett.* **18**, 849 (1993).
- H. Defienne, W. P. Bowen, M. Chekhova, *et al.*, *Nat. Photonics* **18**, 1024 (2024).
- J. Zopes, K. Sasaki, K. Cujia, *et al.*, *Phys. Rev. Lett.* **119**, 260501 (2017).
- W. Luo, L. Cao, Y. Shi, *et al.*, *Light Sci. Appl.* **12**, 175 (2023).
- S. Shi, L. Tian, Y. Wang, *et al.*, *Phys. Rev. Lett.* **125**, 070502 (2020).
- S. Shi, Y. Wang, L. Tian, *et al.*, *Laser Photonics Rev.* **17**, 2200508 (2023).
- M. Tse, H. Yu, N. Kijbunchoo, *et al.*, *Phys. Rev. Lett.* **123**, 231107 (2019).
- F. Acernese, M. Agathos, L. Aiello, *et al.*, (Virgo Collaboration), *Phys. Rev. Lett.* **123**, 231108 (2019).
- A. Buikema, C. Cahillane, G. Mansell, *et al.*, *Phys. Rev. D* **102**, 062003 (2020).
- Y. Zhao, N. Aritomi, E. Capocasa, *et al.*, *Phys. Rev. Lett.* **124**, 171101 (2020).
- J. Lough, E. Schreiber, F. Bergamin, *et al.*, *Phys. Rev. Lett.* **126**, 041102 (2021).
- T. Kashiwazaki, T. Yamashima, K. Enbutsu, *et al.*, *Appl. Phys. Lett.* **122**, 234003 (2023).
- Y. Zhang, M. Menotti, K. Tan, *et al.*, *Nat. Commun.* **12**, 2233 (2021).
- K. McKenzie, N. Grosse, W. P. Bowen, *et al.*, *Phys. Rev. Lett.* **93**, 161105 (2004).
- F. Meylahn, B. Willke, and H. Vahlbruch, *Phys. Rev. Lett.* **129**, 121103 (2022).
- X. Sun, Y. Wang, L. Tian, *et al.*, *Opt. Lett.* **44**, 1789 (2019).
- L. Gao, L.-a. Zheng, B. Lu, *et al.*, *Light Sci. Appl.* **13**, 294 (2024).
- L.-A. Wu, H. Kimble, J. Hall, *et al.*, *Phys. Rev. Lett.* **57**, 2520 (1986).
- R. Slusher, L. Hollberg, B. Yurke, *et al.*, *Phys. Rev. Lett.* **55**, 2409 (1985).
- H. Goto, S. Nakamura, and K. Ichimura, *Opt. Express* **18**, 23763 (2010).
- H. Vahlbruch, M. Mehmet, K. Danzmann, *et al.*, *Phys. Rev. Lett.* **117**, 110801 (2016).
- W. Zhang, J. Wang, Y. Zheng, *et al.*, *Appl. Phys. Lett.* **115**, 181901 (2019).
- S. Schiller, K. Schneider, and J. Mlynek, *J. Opt. Soc. Am. B* **16**, 1512 (1999).
- A. Schönbeck, F. Thies, and R. Schnabel, *Opt. Lett.* **43**, 110 (2018).
- H. Vahlbruch, S. Chelkowski, B. Hage, *et al.*, *Phys. Rev. Lett.* **97**, 011101 (2006).
- A. Khalaidovski, H. Vahlbruch, N. Lastzka, *et al.*, *Class. Quantum Grav.* **29**, 075001 (2012).
- B. Shajilal, O. Thearle, A. Tranter, *et al.*, *Opt. Express* **30**, 37213 (2022).
- E. Oelker, G. Mansell, M. Tse, *et al.*, *Optica* **3**, 682 (2016).
- M. Sayeh, H. R. Bilger, and T. Habib, *Appl. Opt.* **24**, 3756 (1985).
- L. Casperson, *IEEE J. Quantum Electron.* **10**, 629 (1974).
- A. Ashkin, G. Boyd, and J. Dziedzic, *IEEE J. Quantum Electron.* **2**, 109 (1966).
- Q. Wang, L. Tian, W. Yao, *et al.*, *Opt. Express* **27**, 28534 (2019).
- Z. Ma, D. Guo, X. Xu, *et al.*, *Nature* **555**, 94 (2018).